Photoelectron satellite spectroscopy and angular distribution of argon atoms using a monochromatic EUV source based on high-order harmonic generation

B. Hai,[1,2] S. F. Zhang,[1,2,*] M. Zhang,[1,2] B. Najjari,[1] D. P. Dong,[1,2] J. T. Lei,[3] D. M. Zhao,[1,2] and X. Ma[1,2,†]

[1]*Institute of Modern Physics, Chinese Academy of Sciences, Lanzhou 730000, China*

[2]*University of Chinese Academy of Sciences, Beijing 100049, China*

[3]*School of Nuclear Science and Technology, Lanzhou University, Lanzhou 730000, China*

(Received 4 March 2020; revised manuscript received 21 April 2020; accepted 6 May 2020; published 26 May 2020)

Photoelectron satellite spectra and angular distribution of argon atoms were measured in the energy range of 34–43 eV, using a well-developed reaction microscope mounted on a newly built high-order harmonic generation (HHG) extreme ultraviolet (EUV) source. Various satellites were resolved and the angular distribution asymmetry parameters β were determined for both the main lines and the satellites. It is found that our measured β for the $3p$ and $3s$ main lines are in an excellent agreement with previous results. The β parameters measured for most of the satellites are first reported in this energy range, providing benchmark data for testing different theoretical models.

DOI: 10.1103/PhysRevA.101.052706

I. INTRODUCTION

Photoelectron spectroscopy is a powerful tool for studying the electronic structure of atoms and molecules. A photoelectron spectrum usually consists of an intense main line and weak satellite lines, whereas the energies of satellite lines are lower than those of main lines correspondingly, due to the excitation of the residual ions. The presence of photoelectron satellite lines has been considered as a manifestation of electron correlation effects.

Starting from the 1960s, photoelectron satellites have already been extensively studied both experimentally and theoretically. The involved atoms include closed-shell atoms like He, Ne, Ar, Kr, and Xe [1–7] and open-shell atoms such as Li [8] and Sc [9]. For example, using the technique of photoelectron spectrometry, Wuilleumier and Krause [3] studied the photoionization of Ne between 100 and 2000 eV, and determined cross sections for various processes as a function of photon energy. In a later study of Ar, Becker *et al.* [10] extended the photon energy region to near threshold and showed a dramatic increase of satellite intensity towards threshold, which arises from strong interchannel coupling. Recent works focusing on *ns* subvalence shell photoionization of rare-gas atoms have been reviewed by Sukhorukov *et al.* [11].

Meanwhile, the resolving power of photoelectron spectroscopy had been significantly improved by a combination of high-brilliance synchrotron radiation and high resolution electron spectrometers. In a latest work of Yoshii [12], a resolution of about 5 meV was achieved for Xe using threshold photoelectron spectroscopy, and various satellite peaks were resolved for the first time.

On the other hand, studies of the angular distributions of photoelectrons have also been a continuing interest [13–17]. For a linearly polarized photon, the angular distribution of photoelectrons in a dipole approximation can be described by [18]

$$\frac{\partial\sigma(\varepsilon,\theta)}{\partial\Omega} = \frac{\sigma(\varepsilon)}{4\pi}[1+\beta(\varepsilon)P_2(\cos\theta)], \tag{1}$$

where θ is the angle between the electron emission direction and the photon polarization direction, ε is the photoelectron kinetic energy, and P_2 is the second order Legendre polynomial.

By studying the photoelectron satellites in the region of the $3s$ correlational minimum of Ar, Adam *et al.* [13] found that angular distribution asymmetry parameter β was strongly dependent on the total angular momentum of the final ionic states. Langer *et al.* [19] observed satellite lines with β close to -1 which is independent of the photon energy, i.e., parity-unfavored transitions in Ar, and verified the predictions of angular-momentum transfer theory [20]. Moreover, angular distribution of photoelectrons had experimentally proved a sensitive measure of weak perturbations such as relativistic effects [15,16] and nondipole effects in relatively light systems [17].

However, these earlier studies of photoelectron angular distribution have been limited to measure electrons ejected in one single direction at a time [3]. In order to get the angular dependent spectra, these experimental data have to be carefully calibrated for each directions. The development of a reaction microscope [21] since the 1990s enabled kinematically complete measurements. Reaction fragments could be measured for large solid angles up to 4π, meanwhile satisfactory angular resolutions can be achieved. This technique is superior in angular resolved differential cross section measurement and frees us from calibration issues due to the beam intensity

*zhangshf@impcas.ac.cn
†x.ma@impcas.ac.cn

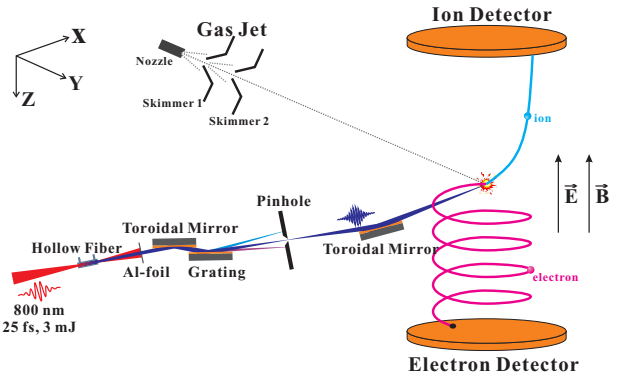

FIG. 1. Schematic experimental setup of the table-top EUV-atom or molecule interactions.

or target density. It thus has been successfully used in fully differential cross section measurements in studies of few-body quantum dynamics in atomic collisions. But, to the best of our knowledge, no application addressing the photoionization satellites has been reported.

In this paper we report kinematically complete measurements of the photoelectron angular distribution for argon using a reaction microscope and a table-top extreme ultraviolet (EUV) source based on monochromatic high-order harmonic generation (HHG). Photoelectrons are collected in 4π solid angle simultaneously which allows the β parameters to be extracted from the fully differential cross sections with much higher accuracy.

II. EXPERIMENTAL SETUP

Photoionization of Ar was studied using a reaction microscope and HHG-based EUV techniques at the Institute of Modern Physics, Chinese Academy of Sciences in Lanzhou. Photoelectron spectra and angular distribution were obtained through momentum imaging for photoelectrons, whose principle is widely reported in literature, e.g., [21]. The schematic of the present experimental setup is shown in Fig. 1.

In brief, EUV photons are produced via high-order harmonic generation processes by focusing intense infrared laser pulses into a 5-cm-long gas-filled hollow fiber with an inner diameter of 150 μm. The driving IR centered at 800 nm is from an ultrafast Ti:sapphire laser system (KMLabs Inc.) and its pulse energy is up to 3 mJ with the pulse duration of 25 fs. Typically, the laser peak intensity is estimated to be around $\sim 10^{14}$ W cm^{-2} inside the fiber. When argon gas is used as a HHG medium, the phase-matched gas pressure inside the fiber is typically about 50 Torr with an input driving pulse energy of 0.6 mJ. Nowadays, highly coherent EUV photon beams can be accessed with table-top HHG technique, which provides us complementary solutions to the conventional large-scale EUV facilities such as synchrotron radiation and free electron laser.

The generated EUV light is first focused by a gold coated toroidal mirror and then diffracted by a flat grating, as shown in Fig. 1. In order to get high reflectivity, both optics operate at a grazing incident angle of about 4 deg. The monochromatic EUV photons were selected through a 150 μm pinhole at

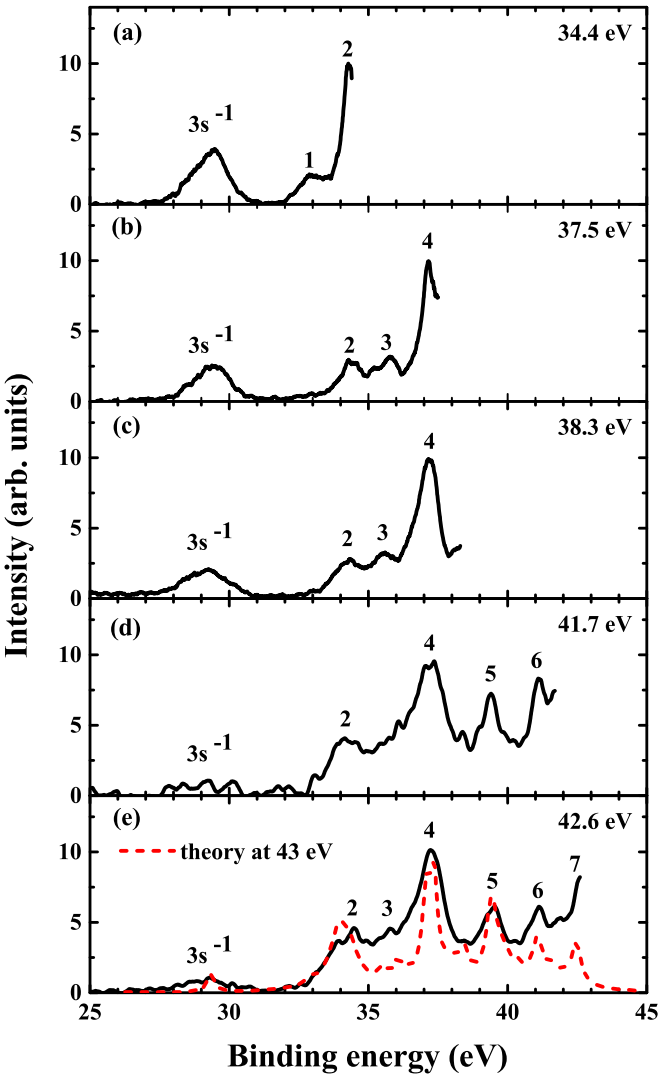

FIG. 2. Photoelectron spectra recorded at different photon energies, the assignments of the peaks are listed in Table I. The dashed red curve shows the theoretical photoelectron spectrum for 43 eV radiation adapted from Sukhorukov *et al.* (1992) [22]. All spectra are normalized to the highest satellite peak [peak 2 in (a) and peak 4 in (b)-(e)], and the $3p^{-1}$ peak is not shown because its intensity is much higher than the satellites.

the focal plane. By switching the pinhole to a CCD camera (Andor DO934P-BN), the energy resolution is measured to be about 0.4 eV for 40 eV incident photon energy. Through the pinhole, the diverging light is then refocused by another toroidal mirror, then enters into an UHV chamber and intersects with the supersonic gas jet at a right angle in the center of the time-of-flight (TOF) spectrometer. The produced recoil ions and photoelectrons are extracted by a weak electrostatic field of $\sim$2 V/cm and detected by two position-sensitive detectors (RoentDek), respectively. Additionally, a homogenous magnetic field of about 10 G is applied to confine the fast-moving photoelectrons and ensure a near-4π collection. With the recorded position and TOF information, three-dimensional momenta of photoelectrons can be reconstructed as well as photoelectron spectra and angular distributions.

TABLE I. Satellite lines observed in this work and assignments of the most prominent states.

	This work		Binding energy from references (eV)		
Peaks	Binding energy (eV)	Assignments	[23]	[24]	[25]
1	33 ± 0.5	$3p^4(^3P)4s\,(^2P)$	32.93	32.900	
2	34.4 ± 0.4	$3p^4(^1D)4s\,(^2D)$	34.24	34.216	34.214
		$3p^4(^3P)3d\,(^2D)$	34.43	34.418	34.417
3	35.4 ± 0.5	$3p^4(^3P)4p\,(^2D)$	35.50	35.442	35.440
		$3p^4(^3P)4p\,(^2P)$	35.66	35.628	35.627
4	37.1 ± 0.5	$3p^4(^1S)4s\,(^2S)$[a]	36.55	36.504	36.504
		$3p^4(^1D)4p\,(^2P)$		37.188	37.112
		$3p^4(^1D)4p\,(^2D)$	37.29	37.261	37.258
		$3p^4(^1D)3d\,(^2D)$	37.18	37.121	37.127
		$3p^4(^1D)3d\,(^2P)$	37.48	37.381	37.384
5	39.4 ± 0.5	$3p^4(^3P)5p\,(^2P)$		39.33	39.330
		$3p^4(^3P)5p\,(^2D)$		39.39	39.380
		$3p^4(^3P)4d\,(^2P)$	39.45	39.39	39.391
		$3p^4(^1S)4p\,(^2P)$		39.57	39.562
		$3p^4(^3P)4d\,(^2D)$	39.70	39.64	39.634
6	41.1 ± 0.3	$3p^4(^3P)5d\,(^2D)$		41.13	
		$3p^4(^3P)5d\,(^2P)$		41.21	
		$3p^4(^1D)4d\,(^2S)$	41.24	41.21	
7	42.5 ± 0.1	$3p^4(^1D)5d\,(^2D)$		42.31	
		$3p^4(^1D)5d\,(^2S)$		42.68	

[a]Only contributes to the shoulder on the lower binding-energy side.

For a given photon energy, the photoelectron kinetic energy equals the photon energy minus the binding energy, mapping the different states of the ion onto peaks in the photoelectron energy spectrum. During the data analysis, by setting conditions to the photoelectron energy, the angular distribution for a specific transition can be obtained.

III. RESULTS AND DISCUSSION

In the following discussions the coordinate system is defined as shown in Fig. 1, with the light propagating direction defined as X axis, the light polarization direction (also is the gas jet direction) as Y, and the TOF direction as Z.

Figure 2 shows the angle integrated binding energy spectra for incident photon energies of 34.4, 37.5, 38.3, 41.7, and 42.6 eV, respectively. The $3s$ main line as well as several satellites were assigned according to the early works of high resolution spectroscopy [10,23–25], as listed in Table I. Besides the $3s^{-1}$ peak, there are seven additional peaks observed in the spectra. However, we were not able to fully resolve all the satellite states due to the limited energy resolution. Every peak corresponds to a composition of few excited states of the Ar^+ ion.

A theoretical spectrum from Sukhorukov *et al.* [22] is also given in Fig. 2(e), for 43 eV incident photon energy (the red dashed curve), where an energy resolution of 0.3 eV was assumed for spectrum convolution. Despite that the characteristic structures of experimental spectrum (black curve) for $E_{ph} = 42.6$ eV have been well reproduced by the theoretical calculations, significant differences can be observed at the highest binding energy side. The abrupt rise toward high binding energy side is due to the enhanced cross sections caused by electron correlations at low photoelectron energy. In fact, similar enhanced cross sections near the photoionization threshold have been observed and ascribed to the electron correlation effects which have been confirmed in many works, for instance see [10,24] and references therein. The underestimation of cross sections near threshold implies that the theory is still far from satisfactory and pose a challenge for theoreticians.

Figure 3(a) represents photoelectron momentum distribution in the plane perpendicular to the Z axis ($|P_z| < 0.1$ a.u.) by incident photon energy of 38.3 eV. The concentric rings

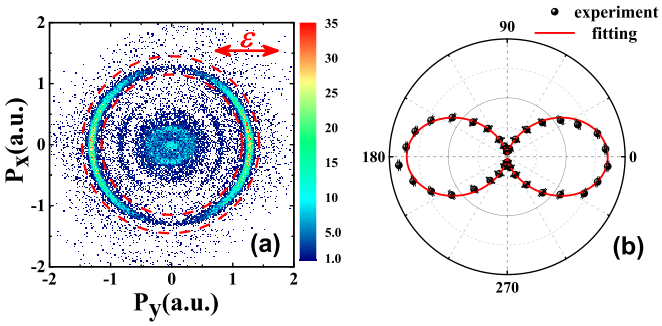

FIG. 3. (a) Photoelectron momentum distribution for 38.3 eV photon energy, in the plane formed by the light polarization (y, as indicated by the arrows) and the light propagating direction (x), for events with transverse momentum $|P_z| < 0.1$ a.u. (b) Angular distribution of the $3p$ photoelectrons [events between the dashed circles in (a)] as a function of the angle between electron momentum and the light polarization. Solid red line shows the fitting by Eq. (1) with $\beta = 1.87 \pm 0.05$.

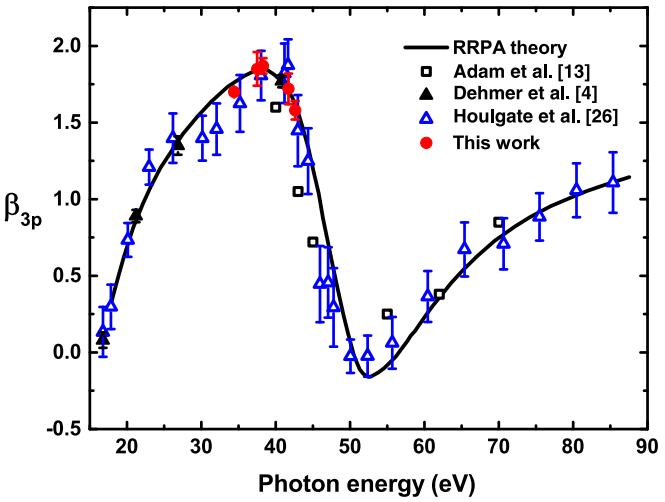

FIG. 4. Angular distribution asymmetry parameter β for the $3p$ ionization of argon, as a function of the photon energy. Experimental data: solid circles, this work; open triangles, Houlgate *et al.* [26]; solid triangles, Dehmer *et al.* [4]; open squares, Adam *et al.* [13]. Solid curve is the relativistic random-phase approximation (RRPA) calculation by Johnson and Cheng [27].

in the figure are corresponding to different photoelectron emission channels. The outmost ring represents $3p$ main line, while inner rings are for $3s$ main line and satellites. The photoelectron angular distribution for $3p$ main line presents an apparent dipole pattern, as shown in Fig. 3(a). By fitting the measured angular distribution to Eq. (1), an asymmetry parameter $\beta = 1.87 \pm 0.05$ was obtained. Since the driving IR has a linearly polarization of more than 99.9% which is guaranteed by an optical polarizer, leading to a high degree of polarization of the HHG, the uncertainty of asymmetry parameters induced by the photon polarization is negligible.

As mentioned already, the advantage of employing a reaction microscope to extract the β parameters from angular distributions is that the systematic uncertainties are much smaller because no calibration on beam intensity or target density are needed. The accuracy of an asymmetric parameter obtained here is thus mainly determined by the statistics and the noise level. Figure 4 shows the measured asymmetry parameters β_{3p} as a function of incident photon energies in comparison with those obtained by other groups. Together with spectra of Fig. 3, one can safely conclude that results obtained from our reaction microscope measurements are reliable. Employing similar methods, asymmetry parameters for resolved lines were obtained and summarized in Table II.

The cross section of Ar $3s$ photoionization has a correlational minimum of only about 0.01 Mb [28] near 42 eV. As a result, the count statistics of $3s$ for 41.7 and 42.6 eV in our experiments are very poor, as can be seen from Figs. 2(d) and 2(e), retrieval of the β parameter for these two energies are thus of no significance. However the background contribution is relatively smaller for the other three energies, and the β parameters we obtained agree with the only two existing measurements within mutual error bars, as illustrated in Fig. 5. The relatively large error bars results from poor statistics due to small cross sections, which could be improved when the HHG EUV source provides higher photon flux after the upgrade.

TABLE II. Line assignments and angular asymmetry parameters β for all resolved peaks. The uncertainties of the last significant number(s) are indicated in the parentheses.

	β at different photon energies				
Peaks	34.4 eV	37.5 eV	38.3 eV	41.7 eV	42.6 eV
	1.70(2)	1.85(11)	1.87(5)	1.72(10)	1.58(6)
	1.98(12)	1.99(14)	1.85(16)		
1	0.04(10)				
2	0.19(9)	−0.10(6)	0.45(7)	1.02(23)	0.94(16)
3		0.42(9)	0.52(5)	0.82(30)	0.86(16)
4		0.09(8)	0.11(2)	0.01(6)	−0.01(4)
5				0.33(11)	0.09(7)
6				−0.18(8)	−0.28(6)
7					0.18(9)

As for the satellite states, only three measurements of β parameter have been reported so far in literature [13,19,30] and the photon energy regions in those works are higher than that in the present work. Moreover, theoretical calculations of β parameter for satellites are also scarce partly due to the lack of experimental data. The data reported here, therefore, could promote studies of relevant fundamental processes by providing the benchmark data near the threshold regime.

According to the calculation of Sukhorukov *et al.* [31] and measurement of Becker *et al.* [10], the cross section for the $3p^4(^3P)4s(^2P)$ satellite decreases very rapidly when the photon energy increases. This explains why peak 1 is only observed for the lowest photon energy in our experiments, and our result of the asymmetry parameter β indicates that the photoelectrons are emitted in an isotropic manner near threshold. Currently it is the only available data for this satellite.

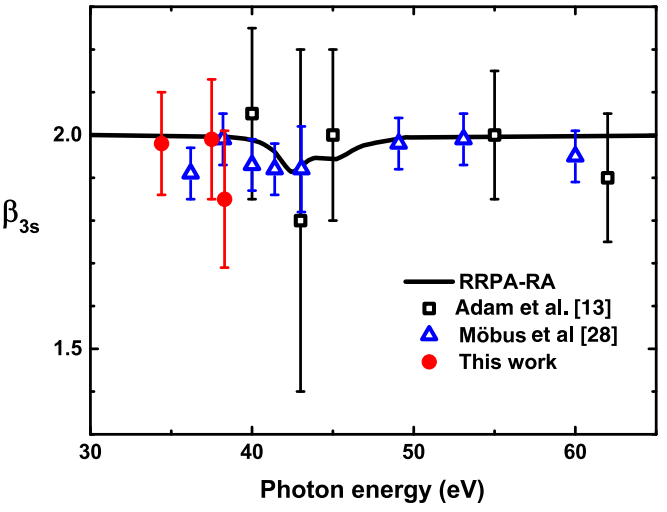

FIG. 5. Angular distribution asymmetry parameter β for the $3s$ ionization of argon, as a function of the photon energy. Experimental data: solid circles, this work; open triangles, Möbus *et al.* [28]; open squares, Adam *et al.* [13]. The solid curve is the calculation from Kutzner *et al.* [29] using relativistic random-phase approximation with relaxation and Auger effect (RRPA-RA).

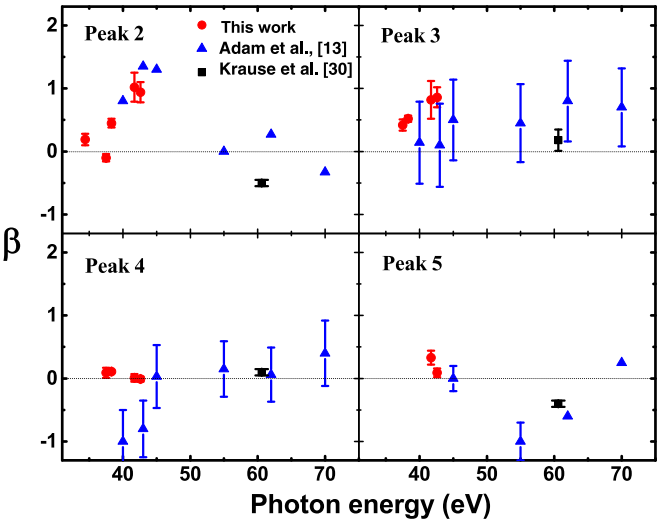

FIG. 6. Comparison of the β parameters of this work with previous results, for satellite peaks 2–5. Experimental data: red solid circles, this work; blue solid triangles, Adam *et al.* [13]; black solid squares, Krause *et al.* [30].

Another interesting case is for peak 6 composed of $3p^4(^3P)5d(^2D,\ ^2P)$ and $3p^4(^1D)4d(^2S)$ which are quasidegenerate but have very special angular features. As discussed in [19], the $3p^4(^3P)5d(^2P)$ satellite should be a parity-unfavored transition which has an energy independent asymmetry parameter β of -1. While the $3p^4(^1D)4d(^2S)$ satellite which arise from the well-known configuration interaction $3s3p^6(^2S) \leftrightarrow 3s^23p^4nd(^2S)$ should have a β value of 2 [30], similar to the $3s$ mainline. Because both of these asymmetry parameters are constant and the contribution of $3p^4(^3P)5d(^2D)$ satellite is negligible due to its relatively rather small cross section near threshold [31], the composite β value is simply determined by the ratio of these two satellites and their corresponding β values. A simple weighting analysis of the measured β value of -0.18 and -0.28 gives the proportion of about 27% and 24% for the $3p^4(^1D)4d(^2S)$ satellite, respectively, consistent with 28% obtained from the cross section data at 43 eV calculated by Sukhorukov *et al.* [31].

On the other hand, for photon energies above 55 eV, the β values measured by Adam *et al.* [13] are close to 2. In such a case this peak can only be assigned to the $3p^4(^1D)4d(^2S)$ satellite. This indicates that the contribution of $3p^4(^3P)5d(^2D,\ ^2P)$ satellites become very small compared with the $3p^4(^1D)4d(^2S)$ satellite at such photon energies, which is also consistent with the cross sections predicted by Sukhorukov *et al.* [31].

For other peaks, the β values obtained in our experiment are presented together with previous results by various authors for different energy regions in Fig. 6. From the figure we see that our data of the β parameters are more accurate (smaller error bars) than those given by Adam *et al.* [13], which clearly show the advantage of the present experimental technique. From each spectrum, one can draw the following conclusions: (i) the β parameters for peak 2 exhibit a similar behavior as for the $3p$ main line shown in Fig. 4. This suggests that peak 2 may arise mainly from the single configuration interaction with the $3s^23p^5(^2P)$ ground state. (ii) Our measured βs for peak 3 and the previous measurements from literature show a small variation as a function of the photon energy, thus for such an energy interval the β parameter for peak 3 is energy independent. (iii) Our measured βs for peak 4 are close to zero and deviate significantly with the values of Adam *et al.* [13] for photon energies below 45 eV. However, our data together with their data given beyond 45 eV as well as the result of Krause *et al.* [30] show an energy independent behavior of the β parameter with averaged values very close to zero. This suggests an isotropic behavior of the cross sections for this peak. (iv) Our result with those from literature show that β parameter for peak 5 exhibits strong photon energy dependence in contrast to peaks 3 and 4.

One has to note that there are still some discrepancies between different experiments. Therefore, further experimental and theoretical investigations are needed for a better understanding of the mechanisms behind these satellite lines and thus remove the doubt engendered by these discrepancies.

IV. CONCLUSION

We have measured the photoelectron satellite spectra and angular distribution of argon atom using a reaction microscope in the energy range near threshold. Seven satellites were resolved and assigned. Our results of the angular distribution asymmetry parameter β for $3p$ and $3s$ main lines agree well with previous measurements reported in literature. The β parameters for all resolved satellites were measured. By analyzing the angular distribution of quasidegenerate satellites, the branch ratio was obtained, which accord closely with theoretical value. Comparison of the measured β parameters with previous results in different energy regions showed very different behaviors for the satellites.

Combinations of the table-top HHG source with the reaction microscope exhibit high potential in investigating fundamental processes such as photoeffects near threshold in a multielectron system where electron correlations play an important role. Further experiments with higher resolution are needed for a better determination of the β parameter for every individual satellite. There is also an urgent need for theoretical calculations of the β parameters for photoionization satellites, in order to have a better understanding of the experimental results.

ACKNOWLEDGMENTS

This work was supported by the National Key Research and Development Program of China (No. 2017YFA0402300) and the NSFC program (Grant No. 11934004).

[1] T. A. Carlson, Phys. Rev. **156**, 142 (1967).
[2] M. Amusia, N. Cherepkov, and L. Chernysheva, Phys. Lett. A **40**, 15 (1972).
[3] F. Wuilleumier and M. O. Krause, Phys. Rev. A **10**, 242 (1974).
[4] J. L. Dehmer, W. A. Chupka, J. Berkowitz, and W. T. Jivery, Phys. Rev. A **12**, 1966 (1975).

[5] P. A. Heimann, C. M. Truesdale, H. G. Kerkhoff, D. W. Lindle, T. A. Ferrett, C. C. Bahr, W. D. Brewer, U. Becker, and D. A. Shirley, Phys. Rev. A **31**, 2260 (1985).
[6] C. E. Brion, K. H. Tan, and G. M. Bancroft, Phys. Rev. Lett. **56**, 584 (1986).
[7] A. Kikas, S. Osborne, A. Ausmees, S. Svensson, O.-P. Sairanen, and S. Aksela, J. Electron Spectrosc. Relat. Phenom. **77**, 241 (1996).
[8] T. A. Ferrett, D. W. Lindle, P. A. Heimann, W. D. Brewer, U. Becker, H. G. Kerkhoff, and D. A. Shirley, Phys. Rev. A **36**, 3172 (1987).
[9] S. B. Whitfield, K. Caspary, T. Myers, M. Bjelland, R. Wehlitz, J. Jiménez-Mier, P. Olalde-Velasco, and M. O. Krause, J. Phys. B **38**, 3273 (2005).
[10] U. Becker, B. Langer, H. G. Kerkhoff, M. Kupsch, D. Szostak, R. Wehlitz, P. A. Heimann, S. H. Liu, D. W. Lindle, T. A. Ferrett, and D. A. Shirley, Phys. Rev. Lett. **60**, 1490 (1988).
[11] V. Sukhorukov, I. Petrov, B. Lagutin, A. Ehresmann, K.-H. Schartner, and H. Schmoranzer, Phys. Rep. **786**, 1 (2019).
[12] H. Yoshii, T. Aoto, Y. Morioka, and T. Hayaishi, J. Phys. B **40**, 2765 (2007).
[13] M. Y. Adam, P. Morin, and G. Wendin, Phys. Rev. A **31**, 1426 (1985).
[14] P. A. Heimann, U. Becker, H. G. Kerkhoff, B. Langer, D. Szostak, R. Wehlitz, D. W. Lindle, T. A. Ferrett, and D. A. Shirley, Phys. Rev. A **34**, 3782 (1986).
[15] N. Berrah, A. Farhat, B. Langer, B. M. Lagutin, P. V. Demekhin, I. D. Petrov, V. L. Sukhorukov, R. Wehlitz, S. B. Whitfield, J. Viefhaus, and U. Becker, Phys. Rev. A **56**, 4545 (1997).
[16] H. Derenbach and V. Schmidt, J. Phys. B **16**, L337 (1983).
[17] O. Hemmers, R. Guillemin, E. P. Kanter, B. Krässig, D. W. Lindle, S. H. Southworth, R. Wehlitz, J. Baker, A. Hudson, M. Lotrakul, D. Rolles, W. C. Stolte, I. C. Tran, A. Wolska, S. W. Yu, M. Y. Amusia, K. T. Cheng, L. V. Chernysheva, W. R. Johnson, and S. T. Manson, Phys. Rev. Lett. **91**, 053002 (2003).
[18] J. Cooper and R. N. Zare, J. Chem. Phys. **48**, 942 (1968).
[19] B. Langer, J. Viefhaus, O. Hemmers, A. Menzel, R. Wehlitz, and U. Becker, Phys. Rev. A **51**, R882 (1995).
[20] D. Dill and U. Fano, Phys. Rev. Lett. **29**, 1203 (1972).
[21] J. Ullrich, R. Moshammer, A. Dorn, R. Dörner, L. P. H. Schmidt, and H. S. Böcking, Rep. Prog. Phys. **66**, 1463 (2003).
[22] V. Sukhorukov, B. Lagutin, H. Schmoranzer, I. Petrov, and K. H. Schartner, Phys. Lett. A **169**, 445 (1992).
[23] L. Medhurst, A. V. Wittenau, R. V. Zee, S. Zhang, S. Liu, D. Shirley, and D. Lindle, J. Electron Spectrosc. Relat. Phenom. **52**, 671 (1990).
[24] S. Cvejanovic, G. W. Bagley, and T. J. Reddish, J. Phys. B **27**, 5661 (1994).
[25] M. Lundqvist, P. Baltzer, L. Karlsson, and B. Wannberg, Phys. Rev. A **49**, 277 (1994).
[26] R. Houlgate, J. West, K. Codling, and G. Marr, J. Electron Spectrosc. Relat. Phenom. **9**, 205 (1976).
[27] W. R. Johnson and K. T. Cheng, Phys. Rev. A **20**, 978 (1979).
[28] B. Möbus, B. Magel, K. H. Schartner, B. Langer, U. Becker, M. Wildberger, and H. Schmoranzer, Phys. Rev. A **47**, 3888 (1993).
[29] M. Kutzner, Q. Shamblin, S. E. Vance, and D. Winn, Phys. Rev. A **55**, 248 (1997).
[30] M. Krause, S. Whitfield, C. Caldwell, J. Z. Wu, P. van der Meulen, C. de Lange, and R. Hansen, J. Electron Spectrosc. Relat. Phenom. **58**, 79 (1992).
[31] V. Sukhorukov, B. Lagutin, I. Petrov, S. Lavrentiev, H. Schmoranzer, and K. H. Schartner, J. Electron Spectrosc. Relat. Phenom. **68**, 255 (1994).